Thermal Effects in Spintronics: Physics and Applications

38

Hiroto Adachi and Sadamichi Maekawa

Contents

Abstract

Recent progress in investigation of the interplay of spin and heat is reviewed. A special emphasis is placed on the newly discovered example of the thermospin phenomenon termed "spin Seebeck effect" which enables the thermal injection

H. Adachi (✉) • S. Maekawa
Advanced Science Research Center (ASRC), Japan Atomic Energy Agency (JAEA), Tokai, Japan

CREST, Japan Science and Technology Agency, Tokyo, Japan
e-mail: adachi.hiroto@jaea.go.jp; maekawa.sadamichi@jaea.go.jp

Y. Xu et al. (eds.), *Handbook of Spintronics*,
DOI 10.1007/978-94-007-6892-5_54

of spin currents from a ferromagnet into attached nonmagnetic metals over a macroscopic scale of several millimeters. The theoretical basis for understanding the spin Seebeck effect is presented, and other thermal spin effects are briefly discussed as well.

Introduction

Investigation of the interplay of spin and heat has a long history. One example can be observed in the thermoelectric phenomena in Kondo systems [1, 2], where the Seebeck coefficient is found to be strongly enhanced [3]. Because the Seebeck coefficient is a measure of the entropy flow in electron systems [4], the larger the internal entropy of a system, the larger its Seebeck coefficient. Recall that the precursor to the low-temperature Kondo singlet formation accompanies a strong hybridization of the localized spins with the conduction electrons. Therefore, the enormous enhancement of the Seebeck effect in Kondo systems can be viewed as a consequence of an extra entropy addition from the localized spins to the conduction electrons. In this way, the interplay of spin and heat manifests itself in a physical quantity such as the Seebeck coefficient.

The interplay of spin and heat has been discussed in the field of spintronics as well. In 1987, Johnson and Silsbee published the seminal theoretical study [5] on the interfacial thermomagnetoelectric effect, in which they considered the generalization of the interfacial thermoelectric effect to include magnetization transport. This study initiated numerous number of studies on thermally driven spin-polarized currents in a heterostructure composed of metallic ferromagnets [6–15]. In the context of modern spintronics, the pure spin current, i.e., a spin current unaccompanied by a charge flow, is quite important because the pure spin current is considered to be free from the noises associated with charge fluctuations. The recent demonstration of a thermally driven pure spin-current injection from a ferromagnet into a nonmagnetic metal [16] or semiconductor [17] is an example of the thermal manipulation of the pure spin current. It is important to note that the "spin-dependent Seebeck effect" plays a crucial role in such metallic (semiconducting) magnetic heterostructures.

In 2008, Uchida et al. demonstrated that when a ferromagnetic film is placed under the influence of a temperature gradient, a spin current is injected from the ferromagnetic film into attached nonmagnetic metals with the signal observed over a macroscopic scale of several millimeters [18]. This phenomenon, termed the spin Seebeck effect, surprised the community because the length scale seen in the experiments was extraordinarily longer than the spin-flip diffusion length of conduction electrons.

While the "spin-dependent Seebeck effect" [16, 17] is described within the framework proposed by Johnson and Silsbee [5], an understanding of the spin Seebeck effect requires several new ideas and notions. In this chapter, the main focus is the spin Seebeck effect, and the basic ideas to understand this intriguing

phenomenon are introduced. In addition, a brief summary of other thermospin phenomena, in which the interplay of spin and heat is of crucial importance, is also presented. The field of thermal spintronics is sometimes called spin caloritronics [19].

Spin Seebeck Effect

Thermal Spin Injection by Localized Spins

Spin Seebeck effect refers to the generation of a spin voltage caused by a temperature gradient in a ferromagnet. Here, the spin voltage is a potential for electrons' spin to drive spin currents. More concretely, when a nonmagnetic metal is attached on top of a material with a finite spin voltage, a nonzero spin injection is obtained. The spin Seebeck effect is now established as a universal aspect of ferromagnets because this phenomenon is observed in various materials ranging from the metallic ferromagnets $Ni_{81}Fe_{19}$ [18] and Co_2MnSi [20], the semiconducting ferromagnet (Ga, Mn)As [21], to the insulating magnets $LaY_2Fe_5O_{12}$ [22] and (Mn, Zn) Fe_2O_4 [23].

Figure 1 shows the experimental setup for the first observation of the spin Seebeck effect in $Ni_{81}Fe_{19}$ [18]. Here, a Pt strip is attached on top of a $Ni_{81}Fe_{19}$ film in a static magnetic field $H_0\hat{z}(\gg$ anisotropy field), which aligns the localized magnetic moment along $\hat{z}$. First, a temperature gradient ∇T is applied along the z-axis, which induces a spin voltage across the $Ni_{81}Fe_{19}$/Pt interface. Then this spin voltage injects a spin current I_s into the Pt strip (or ejects it from the Pt strip). A part of the injected/ejected spin current I_s is converted into a charge voltage through the so-called inverse spin Hall effect [24]:

$$V_{\mathrm{ISHE}} = \Theta_H(|e|I_s)(\rho/w), \tag{1}$$

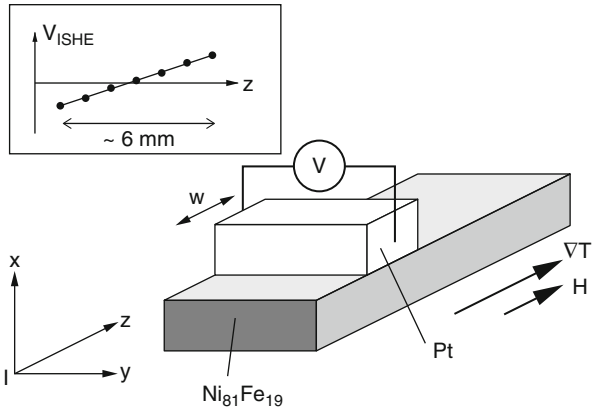

Fig. 1 Schematic of the experimental setup for observing the spin Seebeck effect [18]. Inset: spatial dependence of the observed voltage. The data are measured by changing the position of the Pt strip

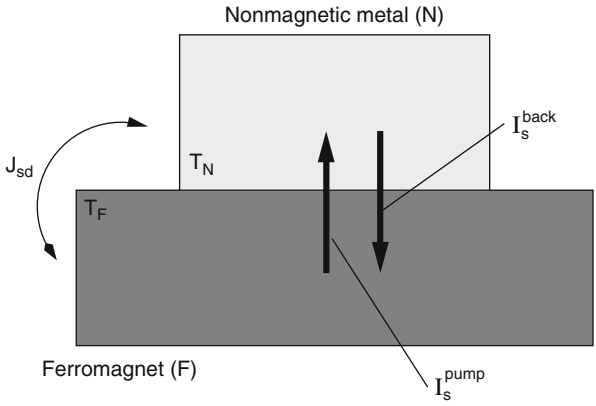

Fig. 2 Side-view schematic of a ferromagnet (F)/nonmagnetic metal (N) junction. $F(N)$ has the local temperature $T_F(T_N)$

where $|e|$, Θ_H, ρ, and w are the absolute value of electron charge, the spin Hall angle, the electrical resistivity, and the width of the Pt strip (see Fig. 1). Hence, the observed charge voltage V_{ISHE} is a measure of the injected/ejected spin current I_s.

As shown in the inset of Fig. 1, the spatial dependence of the spin Seebeck effect can be measured by changing the position of the Pt strip. Note that the signal has a quasi-linear spatial dependence, with the signal changing signs at both ends of the sample and vanishing at the center of the sample.

It has already been shown that the conduction electrons alone cannot explain the spin Seebeck effect, because the conduction electrons' short spin-flip diffusion length (~ several nanometers in a NiFe alloy) fails to explain the long length scale (~ several millimeters) observed in the experiment [25, 26]. This interpretation is further supported by the following two experiments. In Ref. [27], using a ferromagnetic insulator yttrium iron garnet, it was demonstrated that spin currents can be carried by low-lying collective excitations of the localized spins, i.e., spin waves or magnons. Subsequently, it was reported that, despite the absence of the conduction electrons, the spin Seebeck effect can be observed in $LaY_2Fe_5O_{12}$, a magnetic insulator [22]. These experiments suggest that, contrary to the conventional wisdom gathered over the last two decades that the spin current is carried by conduction electrons [28], the magnon is a promising candidate as a carrier for the spin Seebeck effect.

Because the conduction electrons are excluded from the possible scenario for the spin Seebeck effect, the remaining scenario is based on the dynamics of the localized spins in the ferromagnet. To understand the spin Seebeck effect from this viewpoint, it is helpful to first consider the model for the thermal spin injection shown in Fig. 2. In this model, a ferromagnet (F) with the local temperature T_F and a nonmagnetic metal (N) with the local temperature T_N are interacting weakly through interface s-d coupling J_{sd}. For simplicity, it is assumed here that F and N are sufficiently small such that the spatial variations of any physical quantities can be neglected and that the size of the localized spin is unified. It is also assumed

that each segment is initially in local thermal equilibrium; then, the *s*-*d* interactions are switched on, and the nonequilibrium dynamics of the system is calculated.

The physics of the ferromagnet F is described by the localized moment M, for which the dynamics is modeled by the Landau-Lifshitz-Gilbert equation:

$$\frac{d}{dt}\boldsymbol{M} = \left[\gamma(\boldsymbol{H}_{\text{eff}} + \boldsymbol{h}) - \frac{J_{\text{sd}}}{\hbar}\boldsymbol{s}\right] \times \boldsymbol{M} + \frac{\alpha}{M_s}\boldsymbol{M} \times \partial_t \boldsymbol{M}, \tag{2}$$

where H_{eff} is the effective field, γ is the gyromagnetic ratio, α is the Gilbert damping constant, and M_s is the saturation magnetization. In the above equation, the noise field h represents the thermal fluctuations in F, and by the fluctuation-dissipation theorem, it is assumed to obey the following Gaussian ensemble [29]:

$$< h^i(t) >= 0, \tag{3}$$

$$< h^i(t)h^j(t') >= \frac{2k_B T_F \alpha}{\gamma a_S^3 M_s}\delta_{ij}\delta(t-t'), \tag{4}$$

where $a_S^3 = \hbar\gamma/M_s$ is the cell volume of the ferromagnet.

The physics of the nonmagnetic metal N is described by the itinerant spin density $\boldsymbol{s}$, and its dynamics is modeled by the Bloch equation:

$$\frac{d}{dt}\boldsymbol{s} = -\frac{1}{\tau_{\text{sf}}}\left(\boldsymbol{s} - s_0\frac{\boldsymbol{M}}{M_s}\right) - \frac{J_{\text{sd}}}{\hbar}\frac{\boldsymbol{M}}{M_s} \times \boldsymbol{s} + \boldsymbol{l}, \tag{5}$$

where τ_{sf} is the spin-flip relaxation time and $s_0 = \chi_N J_{\text{sd}}$ is the local equilibrium spin density [30] with the paramagnetic susceptibility χ_N in N. In this equation, the noise source l is introduced [31] as a Gaussian ensemble:

$$< l^i(t) >= 0, \tag{6}$$

$$< l^i(t)l^j(t') >= \frac{2k_B T_N \chi_N}{\tau_{\text{sf}}}\delta_{ij}\delta(t-t'), \tag{7}$$

to satisfy the fluctuation-dissipation theorem [32].

From now on, focus is placed on the spin-wave region, where the magnetization M fluctuates only weakly around the ground state value $M_s\hat{\boldsymbol{z}}$ and $\boldsymbol{M}/M_s = \hat{\boldsymbol{z}} + \boldsymbol{m}$ is established to separate small fluctuations m from the ground state value. The spin current I_s induced in the nonmagnetic metal N can be calculated as the rate of change of the spin density in N as $I_s =< \frac{d}{dt}s^z(t) >$. Performing the perturbative approach in terms of J_{sd}, $I_s(t)$ is calculated to be

$$I_s(t) = \frac{J_{\text{sd}}}{\hbar}\mathfrak{Im} < s^+(t)m^-(t') >_{t'\to t} \tag{8}$$

from Eq. 5, where $s^{\pm} = s^x \pm \mathrm{i}s^y$ and $m^{\pm} = m^x \pm \mathrm{i}m^y$. Introducing the Fourier representation $f(t) = \int \frac{d\omega}{2\pi} f_\omega e^{-\mathrm{i}\omega t}$ and employing the fact that the right-hand side of Eq. 8 is only a function of $t - t'$ in the steady state, the following is obtained:

$$I_s = \frac{J_{\mathrm{sd}}}{\hbar} \mathcal{I}\mathrm{m} \int_{-\infty}^{\infty} \frac{d\omega}{2\pi} \ll s_\omega^+ m_{-\omega}^- \gg, \tag{9}$$

where the average $\ll \cdots \gg$ is defined by $\langle s_\omega^+ m_{\omega'}^- \rangle = 2\pi\delta(\omega + \omega') \ll s_\omega^+ m_{-\omega}^- \gg$.

To evaluate the right-hand side of Eq. 9, the transverse components of Eqs. 2 and 5 are linearized with respect to $s_\pm$ and $m_\pm$. Then, to the lowest order in J_{sd}, the following is obtained:

$$s_\omega^+ = \frac{1}{-\mathrm{i}\omega + \tau_{\mathrm{sf}}^{-1}} \left(l_\omega^+ + \frac{s_0 \tau_{\mathrm{sf}}^{-1}}{\omega_0 + \omega - \mathrm{i}\alpha\omega} \gamma h_\omega^+ \right), \tag{10}$$

$$m_\omega^- = \frac{1}{\omega_0 - \omega - \mathrm{i}\alpha\omega} \left(\gamma h_\omega^- + \frac{J_{\mathrm{sd}}}{-\mathrm{i}\omega + \tau_{\mathrm{sf}}^{-1}} l_\omega^- \right), \tag{11}$$

where $\omega_0 = \gamma H_{\mathrm{eff}}$, $h^{\pm} = h^x \pm \mathrm{i}h^y$, and $l^{\pm} = l^x \pm \mathrm{i}l^y$. From the above equations, it is seen that s and m are affected by both the noise field h in F and the noise source l in N through the s-d interaction J_{sd} at the interface. Substituting the above equations into Eq. 9, the spin current injected into N can be expressed as follows:

$$I_s = I_s^{\mathrm{pump}} - I_s^{\mathrm{back}}, \tag{12}$$

where I_s^{pump} and I_s^{back} are respectively defined by

$$I_s^{\mathrm{pump}} = -\frac{J_{\mathrm{sd}} s_0}{\hbar \tau_{\mathrm{sf}}} \int_{-\infty}^{\infty} \frac{d\omega}{2\pi} \frac{\omega}{|\omega - \omega_0 + \mathrm{i}\alpha\omega|^2 |\mathrm{i}\omega - \tau_{\mathrm{sf}}^{-1}|^2} \ll \gamma h_\omega^+ \gamma h_{-\omega}^- \gg, \tag{13}$$

$$I_s^{\mathrm{back}} = -\frac{\alpha J_{\mathrm{sd}}^2}{\hbar^2} \int_{-\infty}^{\infty} \frac{d\omega}{2\pi} \frac{\omega}{|\omega - \omega_0 + \mathrm{i}\alpha\omega|^2 |\mathrm{i}\omega - \tau_{\mathrm{sf}}^{-1}|^2} \ll l_\omega^+ l_{-\omega}^- \gg. \tag{14}$$

It is readily seen in this expression that I_s^{pump} represents the spin current pumped into N by the thermal noise field h in F (the so-called pumping component [33]), while I_s^{back} represents the spin current coming back into F from the thermal noise source l in N (the so-called backflow component [34]). Employing the two fluctuation-dissipation relationships (Eqs. 4 and 6), the pumping and backflow components can be summarized into a single expression:

$$I_s = -\frac{2\alpha\tau_{\mathrm{sf}}^{-1} \chi_N J_{\mathrm{sd}}^2}{\hbar^2} \int_{-\infty}^{\infty} \frac{d\omega}{2\pi} \left(\frac{\omega}{|\omega - \omega_0 + \mathrm{i}\alpha\omega|^2 |\mathrm{i}\omega - \tau_{\mathrm{sf}}^{-1}|^2} \right) k_{\mathrm{B}} (T_F - T_N), \tag{15}$$

where $v_S M_s = \hbar\gamma$ is employed. Using the condition $\tau_{\rm sf}^{-1} \gg \omega_0$ and performing the ω integration, the following is finally obtained:

$$I_s = -G_s \frac{k_{\rm B}}{\hbar}(T_F - T_N), \tag{16}$$

where $G_s = J_{\rm sd}^2 \chi_N \tau_{\rm sf}/\hbar$ is introduced and the negative sign before G_s arises from defining the positive direction of I_s. Interestingly, when the z component of $< \boldsymbol{m} \times \frac{d}{dt}\boldsymbol{m} >$ is calculated from Eq. 2, it can be shown that the pumping component can be expressed as $I_s^{\rm pump} = -G_s < \left[\boldsymbol{m} \times \frac{d}{dt}\boldsymbol{m}\right]^z >$. This expression means that the thermal spin injection into N can be calculated based on the Landau-Lifshitz-Gilbert equation (Eq. 2). The backflow component $I_s^{\rm back}$, which must be subtracted from $I_s^{\rm pump}$ to evaluate the net spin injection, can be obtained by calculating $I_s^{\rm pump}$ at *local thermal equilibrium*. This procedure was used in Ref. [35] to perform the numerical simulation on the spin Seebeck effect.

Equations 12 and 16 indicate that when both F and N are in local thermal equilibrium (i.e., $T_F = T_N$), there is no net spin injection into the attached nonmagnetic metal N. However, conversely, that means that if the ferromagnet F deviates from the local thermal equilibrium for some reason, a finite spin current is injected into (or ejected from) the attached nonmagnetic metal N. This consideration leads to the following simple picture for the spin Seebeck effect. Namely, the essence of the spin Seebeck effect is that the localized spins in the ferromagnet are excited by the heat current flowing through the ferromagnet, which then generate finite spin injections because of the imbalance between the pumping component $I_s^{\rm pump}$ and the backflow component $I_s^{\rm back}$. It is important to note here that the heat current that excites the localized spins has two contributions: the magnon heat current and the phonon heat current. Accordingly, there are two relevant processes in the spin Seebeck effect. The first, in which the localized spins are excited by the magnon heat current, corresponds to the magnon-driven spin Seebeck effect discussed in Refs. [36, 37]. The second, in which the localized spins are excited by the phonon heat current, corresponds to the phonon-drag spin Seebeck effect discussed in Ref. [38]. Note that for these two processes to occur, the *s-d* exchange interaction $J_{\rm sd}$ at the *F*/*N* interface is indispensable.

Magnon-Driven Spin Seebeck Effect and the Concept of Effective Temperature

In the magnon-driven spin Seebeck effect, the localized spins in the ferromagnet are excited by the magnon heat current flowing through the ferromagnet, thereby producing a nonzero spin injection into the attached nonmagnetic metal. This process is considered to be relevant to the "spin Seebeck insulator" [22], where the spin Seebeck effect is observed in an insulating magnet $LaY_2Fe_5O_{12}$ despite the

absence of the conduction electrons. Here, the magnon damping is sufficiently weak such that the long-range magnon propagation may be possible. To date, two approaches to this process have been proposed; one is based on scattering theory, [36] and the other is based on linear-response theory [37]. While both describe the same physics in principle, there are a few differences in detail, particularly in the definition and interpretation of the effective temperature. This difference mainly originates from the assumptions of the two approaches; the linear-response approach considers the deviation from the *local equilibrium* conditions following the standard argument of the linear response [32], whereas the scattering approach considers the deviation from the *global equilibrium* conditions with a uniform temperature distribution [39]. Here, the basic ideas regarding the linear-response formulation given in Ref. [37] are discussed. Note that in Ref. [37], a calculation in terms of the quantum action was presented, which is consistent with the stochastic Landau-Lifshitz-Gilbert equation (Eq. 2) combined with the Bloch equation (Eq. 5). An example of the correspondence between the effective action formulation and the stochastic model formulation can be seen in Ref. [40].

Consider the model shown in Fig. 3, where the ferromagnet (F) and the nonmagnetic metals (N) are divided into three temperature domains of F_1/N_1, F_2/N_2, and F_3/N_3. An important point in this model is that there is no temperature difference between the ferromagnet and the attached nonmagnetic metals, i.e., $T_{N_1} = T_{F_1} = T_1, T_{N_2} = T_{F_2} = T_2$, and $T_{N_3} = T_{F_3} = T_3$. As before, it is assumed that each domain is initially in local thermal equilibrium without interactions with the neighboring domains. The interactions are then switched on among the domains, and the nonequilibrium dynamics of the system is calculated. Here and hereafter, the diagrammatic representation of each elementary process [41] is used. In Fig. 3a, the thin solid lines with arrows (bold lines without arrows) represent the electron propagators (magnon propagators).

First, consider the process P_1 shown in Fig. 3a, where the magnons travel around the ferromagnet F_1 without sensing the temperature difference between F_1 and F_2. This situation corresponds to the process discussed in the previous subsection, and the condition $T_{N_1} = T_{F_1}$ results in zero spin injection (see Eq. 16), which means that, through the "local" process P_1 shown in Fig. 3a, the spin current is *not* injected into the nonmagnetic metal N_1 when F_1 and N_1 have the same temperature. That is, the "local" process cannot explain the experimental results obtained when no temperature difference exists between the ferromagnetic film and the attached Pt film. To account for these results, it is necessary to next consider the process P_1' in Fig. 3a, in which magnons sense the temperature difference between F_1 and F_2. In this case, the magnons deviate from the local thermal equilibrium condition because they sense not only the temperature T_1 but also the temperature T_2 and produce a finite spin injection. Evaluating the diagram P_1' by making use of the procedure as in the previous subsection, the spin Seebeck signal is calculated to be [37]:

$$I_s = G_s \omega_0 \tau_{\mathrm{m}} \frac{k_{\mathrm{B}}(T_1 - T_2)}{\hbar(\Lambda/a_S)} = G_s \omega_0 \tau_{\mathrm{m}} \frac{k_{\mathrm{B}}}{\hbar} a_S \nabla T, \tag{17}$$

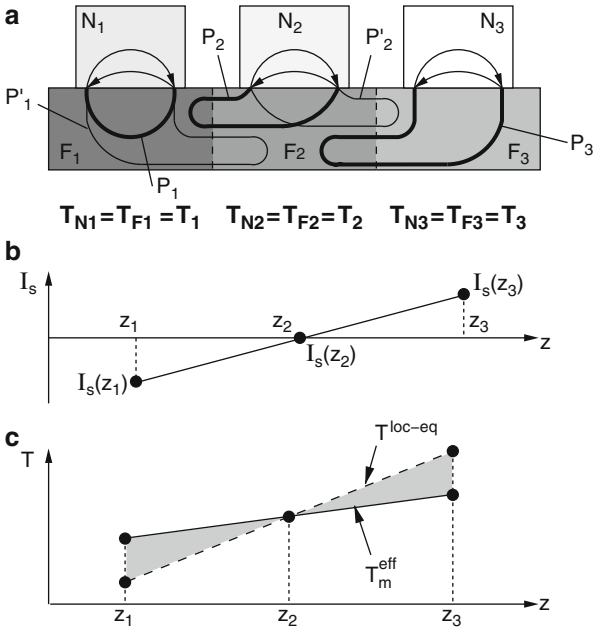

Fig. 3 (**a**) System composed of a ferromagnet (F) and nonmagnetic metals (N) divided into the three temperature domains of F_1/N_1, F_2/N_2, and F_3/N_3 with local temperatures of T_1, T_2, and T_3, respectively. The *thin solid lines* with *arrows* (*bold lines* without *arrows*) represent electron propagators (magnon propagators). (**b**) Spatial profile of the spin currents induced in nonmagnetic metals. (**c**) Spatial profile of the "effective" magnon temperature $T_{\rm m}^{\rm eff}$ and local equilibrium temperature $T^{\rm loc-eq}$. Because the spin accumulation in the nonmagnetic metal senses the local equilibrium temperature $T^{\rm loc-eq}$, the spin Seebeck effect picks up the temperature difference between $T^{\rm loc-eq}$ and $T_{\rm m}^{\rm eff}$ (the *shaded area*)

where Λ is the size of the ferromagnet along the temperature gradient. Note that the signal is proportional to the magnon lifetime $\tau_{\rm m} = 1/(\alpha\omega_0)$, because the carriers of the heat current in this process are magnons. The spin current $I_s(z_3)$ injected into the right terminal N_3 can be calculated in the same manner by considering the process P_3, which gives $I_s(z_3) = -I_s(z_1)$ because of the relationship $T_1 - T_2 = -(T_3 - T_2)$. The spin current $I_s(z_2)$ injected into the middle terminal N_2 vanishes because the two relevant processes (P_2 and P_2') cancel out. Therefore, the spatial profile of the injected spin current is obtained as shown in Fig. 3b. Note that the effects from the spatial variations in the magnetization $\boldsymbol{M}[T(\boldsymbol{r})]$ through the local temperatures $T(\boldsymbol{r})$ are considered in this treatment, because the temperature dependence of M in the magnon region is automatically described by the number of thermal magnons discussed here.

To gain an intuitive understanding of the results obtained above, it is very useful to introduce the concept of effective temperature, which characterizes the nonequilibrium state. The key in the present discussion is the existence of a local thermal equilibrium temperature $T^{\rm loc-eq}$ that can be identified, for example, as the

temperature of *optical* phonons having a localized nature with a large specific heat but small thermal conductivity. Note that most of the phonon heat current is carried by *acoustic* phonons. The present definition of the effective temperature employs the idea discussed by Hohenberg and Shraiman [42], in which the distribution function of a nonequilibrium state is mimicked by a distribution function of an approximate equilibrium state with an effective temperature. Then, the effective temperature in a *nonequilibrium* system is defined by the following relationship:

$$T_{\mathrm{m}}^{\mathrm{eff}} = \lim_{q \to q_0} \frac{C(q, t=0)}{R_s(q)}, \tag{18}$$

where $C(q, t=0)$ is the equal-time correlation function of magnons, $R_s(q)$ is the static response function of the magnons calculated from the dynamic response function $R(q, \omega)$ as $R_s(q) = \mathcal{P}\int \frac{d\omega}{\pi} \mathcal{I}\mathrm{m}R(q,\omega)/\omega$ with $\mathcal{P}$ denoting the principal value [43], and q_0 is the inverse of the thermal de Broglie length.

First, consider the magnons in process P_1, where the magnons sense only the temperature T_1 and stay in the local equilibrium condition. The corresponding response function is given by $R(q,\omega) = \left(\omega - \omega_q - \mathrm{i}\alpha\omega\right)^{-1}$, and through the fluctuation-dissipation relationship, $C(q,\omega) = (2T_1/\omega)\mathcal{I}\mathrm{m}R(q,\omega)$ is given. In this situation, the effective magnon temperature (Eq. 18) coincides with the local equilibrium temperature T_1. Next, consider the process P_1', where the magnons sense not only the temperature T_1 but also the temperature T_2. As expected, the effective magnon temperature in F_1 becomes the linear combination of T_1 and T_2 as

$$T_{\mathrm{m}}^{\mathrm{eff}}(z_1) = (1-r)T_1 + rT_2, \tag{19}$$

where $r \sim \alpha^{-1}(a_S/\Lambda)$. In the same manner, the effective magnon temperature in F_3 is given by $T_{\mathrm{m}}^{\mathrm{eff}}(z_3) = (1-r)T_3 + rT_2$. Finally, the effective magnon temperature in F_2 is not renormalized (i.e., $T_{\mathrm{m}}^{\mathrm{eff}}(z_2) = T_2$) because of the cancelation of the two processes P_2 and P_2'.

These results are summarized in Fig. 3c. Here, $T_{\mathrm{m}}^{\mathrm{eff}}$ is the effective magnon temperature, and $T^{\mathrm{loc-eq}}$ is the local equilibrium temperature that can be identified as the temperature of the localized (optical) phonons modeled by Einstein phonons. The spin accumulation in the nonmagnetic metal senses the local equilibrium temperature $T^{\mathrm{loc-eq}}$ because the nonmagnetic metal is isolated and not extended in the direction parallel to the temperature gradient. Therefore, this effective temperature difference between $T^{\mathrm{loc-eq}}$ and $T_{\mathrm{m}}^{\mathrm{eff}}$ produces the thermal spin injection following Eq. 16. In other words, the spin Seebeck effect picks up the difference in the effective temperature corresponding to the shaded area in Fig. 3c.

Phonon-Drag Spin Seebeck Effect

At the end of section "Thermal Spin Injection by Localized Spins," it was discussed that the heat current flowing through the ferromagnet excites the localized spins, which then causes the spin Seebeck effect. Moreover, it was pointed out that there are two relevant processes underlying the spin Seebeck effect, because both magnon and phonon heat currents can excite localized spins. The latter, in exciting the localized spins and producing finite thermal spin injection, gives rise to the phonon-drag contribution to the spin Seebeck effect [38].

Again, a diagrammatic representation of the elementary process is used. Consider first the process P_1 in Fig. 4a. In this process, the magnons themselves do not sense the temperature difference between T_1 and T_2 but interact with phonons that sense the temperatures T_1 and T_2 and fall into nonequilibrium. These nonequilibrium phonons disturb the local equilibrium conditions of the magnons in F_1 and cause finite spin injection into the nonmagnetic metal N_1.

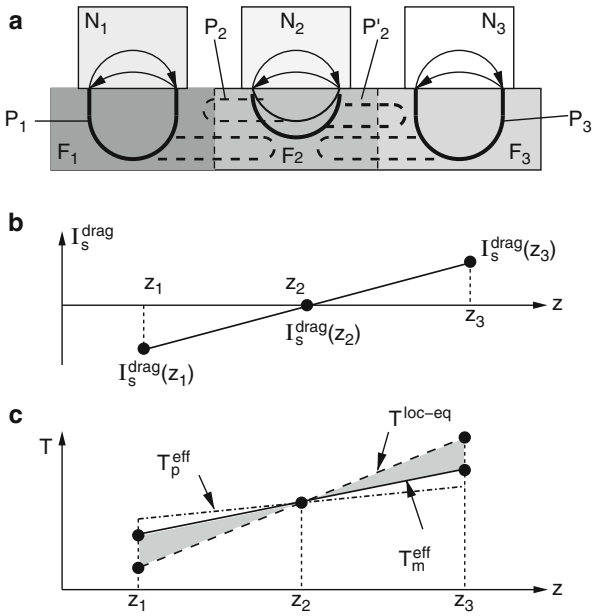

Fig. 4 Diagrammatic representation of the contribution of phonon drag to the spin Seebeck effect. (**a**) Phonon-drag process. The *dashed line* represents a phonon propagator. The meanings of the other lines are the same as those in Fig. 3. (**b**) Spatial profile of the spin currents induced in nonmagnetic metals by the phonon-drag process. (**c**) Spatial profile of the effective magnon temperature $T_{\mathrm{m}}^{\mathrm{eff}}$, the effective phonon temperature $T_{\mathrm{p}}^{\mathrm{eff}}$, and the local equilibrium temperature $T^{\mathrm{loc-eq}}$ in the phonon-drag process. The spin Seebeck effect picks up the temperature difference $T^{\mathrm{loc-eq}}$ and $T_{\mathrm{m}}^{\mathrm{eff}}$ (the *shaded area*)

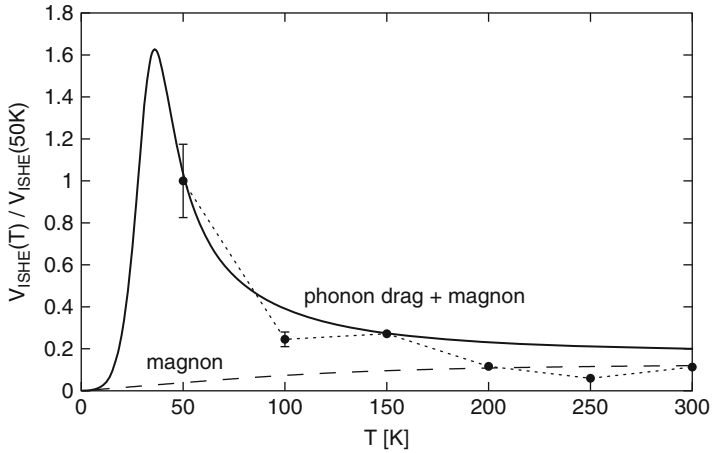

Fig. 5 Temperature dependence of the spin Seebeck effect in $LaY_2Fe_5O_{12}$ [38]. The *solid circles* show the experimental data, and the *solid curve* represents the theoretical fit to the experimental data. The *dashed curve* represents results based on the magnon-driven spin Seebeck effect

This process gives a thermal spin injection with the strength

$$I_s^{\mathrm{drag}} = G_{\mathrm{spin}}\Gamma_{\mathrm{m-p}}^2\left(\frac{\tau_{\mathrm{p}}}{\tau_{\mathrm{sf}}}\right)B\frac{k_{\mathrm{B}}}{\hbar}a_S\nabla T, \tag{20}$$

where $\Upsilon_{\mathrm{m-p}}$ is the effective magnon-phonon coupling constant and τ_{p} is the phonon lifetime. In the above equation, B is given by $B = B_1 \cdot B_2$ with $B_1 = (T/T_D)^{5/4}$ $\int_0^{T_D/T} \frac{du}{4\pi^3}\, u^6/\sinh^2\left(\frac{u}{2}\right)$ and $B_2 = (T/T_M)^{9/2}\int_0^{T_M/T} \frac{dv}{2\pi^2} v^{7/2}/(e^v - 1)$, where T_D is the Debye temperature and T_M is the temperature corresponding to the high-energy magnon cutoff.

The important point of Eq. 20 is that the spin Seebeck signal due to phonon drag is proportional to the phonon lifetime τ_{p}, because the carriers of the heat current in this process are phonons. Because it is well known that the phonon lifetime is strongly enhanced at low temperatures (typically below 100 K) due to a rapid suppression of the Umklapp scattering, Eq. 20 suggests that the spin Seebeck effect is enormously enhanced at low temperatures. In contrast, the signal at zero temperature should vanish because of the third law of thermodynamics. Therefore, the phonon-drag spin Seebeck effect must have a pronounced peak at low temperatures (see Fig. 5 and discussion below). Note that although the possibility of the similar enhancement of the magnon lifetime in the magnon-driven spin Seebeck effect (Eq. 17) is not conclusively excluded, judging from the ferromagnetic resonance linewidth in $Y_3Fe_5O_{12}$ [44] as a measure of the inverse magnon lifetime, it does not seem to be the case.

As in the case of the magnon-driven spin Seebeck effect, the spin current $I_s^{\mathrm{drag}}(z_3)$ injected into the right terminal N_3 can be calculated by considering the process P_3, which gives $I_s^{\mathrm{drag}}(z_3) = -I_s^{\mathrm{drag}}(z_1)$ because of the relationship $T_1 - T_2 = -(T_3 - T_2)$. The spin current $I_s^{\mathrm{drag}}(z_2)$ injected into the middle terminal N_2 vanishes because the two relevant processes (P_2 and P_2') cancel out. Therefore, the spatial profile of the injected spin current can be obtained, as shown in Fig. 4b.

For an intuitive understanding of the phonon-drag spin Seebeck effect, the notion of the effective temperature is again quite useful. As before, the strength of the thermal spin injection is proportional to the difference between the effective magnon temperature $T_{\mathrm{m}}^{\mathrm{eff}}$ and the local thermal equilibrium temperature $T^{\mathrm{loc-eq}}$. But in this case, the deviation of $T_{\mathrm{m}}^{\mathrm{eff}}$ from $T^{\mathrm{loc-eq}}$ is caused by nonequilibrium phonons that push the magnons away from the local thermal equilibrium conditions through the magnon-phonon interaction. Repeating the same argument as in the previous section, the effective magnon temperature $T_{\mathrm{m}}^{\mathrm{eff}}$ and phonon temperature $T_{\mathrm{p}}^{\mathrm{eff}}$ can be obtained, as shown in Fig. 4c. Note that the effective phonon temperature has a smaller slope than the effective magnon temperature because acoustic phonons usually have a greater thermal conductivity. Note, also, that the spin accumulation in the nonmagnetic metal senses the local equilibrium temperature $T^{\mathrm{loc-eq}}$ and does not equilibrate with the effective phonon temperature $T_{\mathrm{p}}^{\mathrm{eff}}$, because the nonmagnetic metal is isolated and does not extend in the direction parallel to the temperature gradient. Therefore, the spin Seebeck effect picks up the difference in the effective temperature corresponding to the shaded area in Fig. 4c. One must also take note that the discussion by Sanders and Walton [39] does not consider the phonon-drag process.

To date, there have been two experimental findings that support the existence of the phonon-drag spin Seebeck effect. The first is the observation of the predicted low-temperature peak in the temperature dependence of the spin Seebeck effect [45, 46]. In Ref. [38], the earliest experimental data on the spin Seebeck effect in $LaY_2Fe_5O_{12}$ were theoretically analyzed, and the theory predicted that the spin Seebeck effect must show a pronounced peak at low temperatures as is discussed above. In Ref. [45], the temperature dependence of the spin Seebeck effect was measured in (Ga, Mn)As, and the data showed a pronounced peak at low temperatures consistent with the theory prediction [38]. In Ref. [46], the same trend was confirmed for yttrium iron garnet. The other experimental finding that supports the scenario of the phonon-drag spin Seebeck effect is the observation of a spin Seebeck effect that is unaccompanied by a global spin current. In Ref. [21], by cutting the magnetic coupling in (Ga, Mn)As while maintaining the thermal contact, it was demonstrated that the spin Seebeck effect can be observed even in the absence of global spin current flowing through (Ga, Mn)As. The scenario of the phonon-drag spin Seebeck effect can explain the "scratch" test experiment as is shown in Fig. 6a, although the idea of a magnon-driven spin Seebeck fails to explain the experiment. Moreover, a recent study [47], in which an *isolated* $Ni_{81}Fe_{19}$ on top of a sapphire substrate was used to measure the spin Seebeck effect (Fig. 6b), excluded the possibility of a dipole-magnon-driven spin Seebeck effect

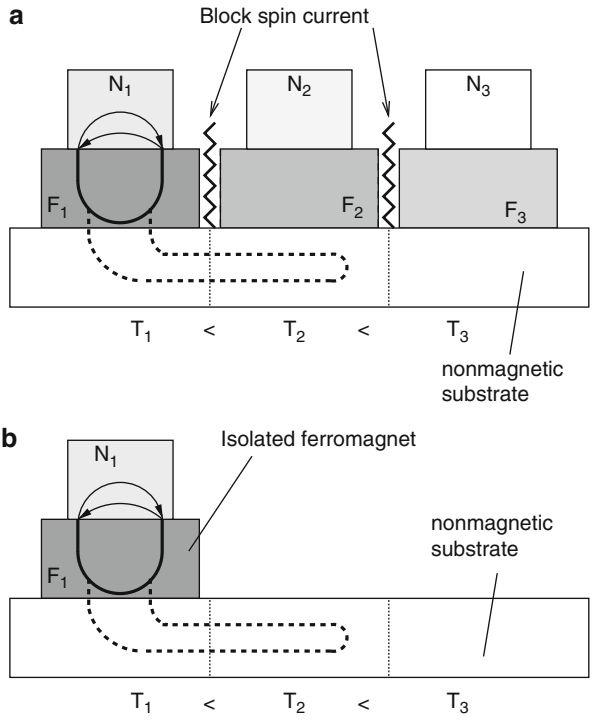

Fig. 6 Diagrammatic representation of the phonon-drag spin Seebeck effect caused by the substrate phonons. This spin Seebeck effect is unaccompanied by a global spin current. (**a**) "Scratch" test experiment in Ref. [21]. (**b**) Observation of the spin Seebeck effect using the "isolated" ferromagnet in Ref. [47]

for the "scratch test" experiment [21] and confirmed that only the phonon-drag process by the substrate phonons can explain the experiment. One important point is that the latter experiment [47] was performed at room temperature; nevertheless, the spin Seebeck effect was observed with the signal extended over several millimeters, as in the first observation of the spin Seebeck effect in $Ni_{81}Fe_{19}$ [18]. This result indicates that the phonon-drag process can contribute to the spin Seebeck effect even at room temperature.

Longitudinal Spin Seebeck Effect

Up to this point, the *transverse* spin Seebeck effect (Fig. 7a), in which the direction of the thermal spin injection into a nonmagnetic metal is *perpendicular* to the temperature gradient, has been discussed. There is another type of spin Seebeck effect called the *longitudinal* spin Seebeck effect [23, 48] (Fig. 7b), in which the direction of the thermal spin injection into a nonmagnetic metal is *parallel* to the temperature gradient. While both *conducting* and *insulating* ferromagnets can be used for the transverse spin Seebeck effect, the longitudinal spin Seebeck effect is well defined only for the use of an *insulating* ferromagnet. This limitation is because, if a *metallic* ferromagnet is used in the case of the

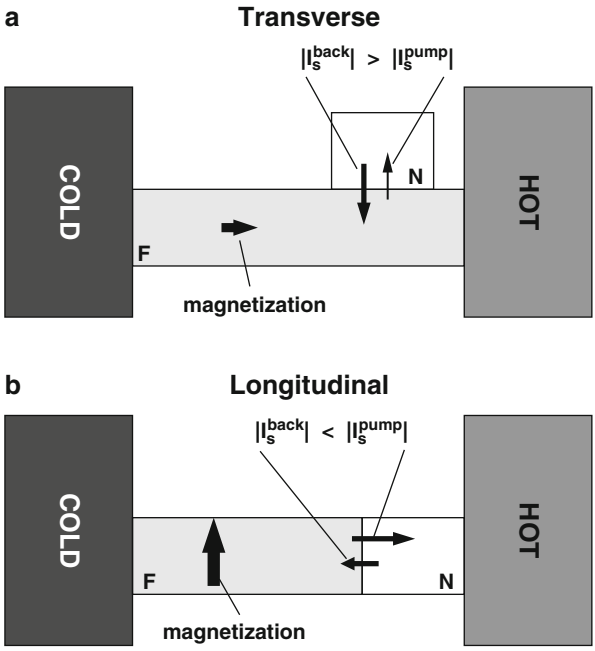

Fig. 7 Schematic of the experimental setup for (**a**) the transverse spin Seebeck effect and (**b**) the longitudinal spin Seebeck effect. When focus is placed on the spin current injected into the nonmagnetic metal (N) close to the hot reservoir, I_s^{pump} is greater than I_s^{back} in the case of the transverse spin Seebeck effect, whereas I_s^{pump} is lesser than I_s^{back} in the case of the longitudinal spin Seebeck effect

longitudinal spin Seebeck effect, the signal is contaminated by the anomalous Nernst effect. The longitudinal spin Seebeck effect has been observed in single crystal [48] and polycrystalline [46] yttrium iron garnet as well as in polycrystalline ferrite (Mn, Zn)Fe_2O_4 [23]. The longitudinal spin Seebeck effect is the simplest configuration in which a bulk polycrystalline ferromagnet can be used. Therefore, it is considered to be a prototype of the spin Seebeck effect from an application viewpoint.

One of the pronounced features of the longitudinal spin Seebeck effect is that the sign of the spin injection is opposite [23, 48] to that in the transverse spin Seebeck effect. As shown in Fig. 7, when focus is placed on the spin current injected into the nonmagnetic metal (N) close to the hot reservoir, the magnitude of the pumping component I_s^{pump} is less than the backflow component in I_s^{back} in the case of the transverse spin Seebeck effect. In contrast, the magnitude of I_s^{pump} is greater than I_s^{back} in the case of the longitudinal spin Seebeck effect. Note that magnons carry spin minus 1, such that the pumping and backflow components have a negative sign.

The sign reversal in the signal between the longitudinal and the transverse spin Seebeck effect can be interpreted in the following way [49]. First, recall that the spin Seebeck effect can be understood in terms of the imbalance between the thermal noise of the magnons in the ferromagnet and the thermal noise of the conduction-electron spin density in the nonmagnetic metal, as seen in Eq. 12. The former noise injects the spin current into the nonmagnetic metal, while the latter ejects the spin current from the nonmagnetic metal. Because the thermal noise

in each element can be related to its effective temperature through the fluctuation-dissipation theorem, the spin Seebeck effect can also be interpreted in terms of the imbalance between the effective temperature of the magnons in the ferromagnet and the effective temperature of the conduction-electron spin density in the nonmagnetic metal (see Eq. 16).

Then, the sign reversal in the signal between the longitudinal spin Seebeck effect and the transverse one may be explained on the basis of the following conditions: (i) most of the heat current in the ferromagnet/nonmagnetic metal hybrid system at room temperature is carried by phonons (see discussion in Ref. [50] in the case of yttrium iron garnet), and (ii) the interaction between the phonons and the conduction-electron spin density in the nonmagnetic metal (N) is much stronger than the magnon-phonon interaction in the ferromagnet (F). In the longitudinal spin Seebeck experiment, the nonmagnetic metal is in direct contact with the heat bath and thereby is exposed to the flow of the phonon heat current due to condition (i). Then, because of condition (ii), conduction-electron spin density in the nonmagnetic metal N is cooled down faster than the magnons in the ferromagnet F, and the resultant effective temperature of the conduction-electron spin density in the nonmagnetic metal decreases below that of the magnons in the ferromagnet (F). In the conventional spin Seebeck setup, by contrast, the nonmagnetic metal N is out of contact with the heat bath, and the phonon heat current does not flow through the nonmagnetic metal N, while the ferromagnet F is in contact with the heat bath, resulting in a decrease in the effective magnon temperature in the ferromagnet F. Therefore, in this case, the effective temperature of the conduction-electron spin density in the nonmagnetic metal N is higher than that of the magnons in the ferromagnet F. This difference may explain the sign reversal of the spin Seebeck effect signal between the longitudinal setup and the conventional setup.

Other Thermal Spin Effects

Up to this point, the discussion is focused on the theoretical aspects of the spin Seebeck effect. In addition to the spin Seebeck effect, there are, of course, several other phenomena in which the interplay of spin and heat is of crucial importance. In this section, the recent progress in this direction is presented.

Spin Injection Due to the Spin-Dependent Seebeck Effect and the Reciprocal Process

A thermally driven pure spin-current injection across a charge-conducting interface has recently been reported by several groups, in which the "spin-dependent Seebeck effect" plays an important role.

Slachter et al. [16] demonstrated the thermally driven pure spin-current injection and its electrical detection using the nonlocal lateral geometry of $Ni_{80}Fe_{20}$/Cu

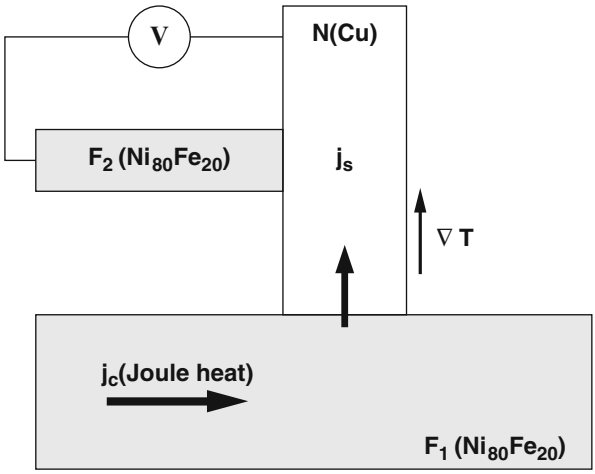

Fig. 8 Schematic of the thermally driven pure spin-current injection device proposed in Ref. [16]. A charge current flowing through the ferromagnet F_1 generates Joule heat and drives the thermal spin-current injection from F_1 into the nonmagnetic metal N

(see Fig. 8). The basic physics behind this experiment is explained by the spin-dependent thermoelectric effect. The spin-dependent current $\boldsymbol{j}_{\uparrow,\downarrow}$ is described by

$$\boldsymbol{j}_{\uparrow,\downarrow} = \sigma_{\uparrow,\downarrow}\left(\frac{1}{e}\nabla\mu_{\uparrow,\downarrow} + S_{\uparrow,\downarrow}\nabla T\right), \tag{21}$$

where $\sigma_{\uparrow,\downarrow}$, $\mu_{\uparrow,\downarrow}$, and $S_{\uparrow,\downarrow}$ are the spin-dependent conductivity, the spin-dependent electrochemical potential, and the spin-dependent Seebeck coefficient, respectively. The spatial distribution of the spin accumulation $\mu_\uparrow - \mu_\downarrow$ is described by the Valet-Fert spin diffusion equation:

$$\nabla^2(\mu_\uparrow - \mu_\downarrow) = \frac{1}{\lambda^2}(\mu_\uparrow - \mu_\downarrow), \tag{22}$$

where λ is the spin-flip diffusion length. The essential feature of the experiment can be captured by solving these two equations under an appropriate temperature distribution across the $Ni_{80}Fe_{20}$/Cu interface.

Le Breton et al. [17] demonstrated the thermal spin injection from $Ni_{80}Fe_{20}$ into Si through an insulating tunnel barrier SiO_2/Al_2O_3 and called the phenomenon "Seebeck spin tunneling" (Fig. 9). Here, the injected spin current was detected by the Hanle effect, and the observed signal was analyzed in terms of the "spin-dependent Seebeck effect." It is important to note that the direction of the spin injection in these two experiments is parallel to the temperature gradient, such that the signal could contain the contribution from the longitudinal spin Seebeck effect discussed in section "Longitudinal Spin Seebeck Effect."

From the Kelvin relation $\Pi_{\uparrow,\downarrow} = TS_{\uparrow,\downarrow}$ with the spin-dependent Peltier coefficient $\Pi_{\uparrow,\downarrow}$, the reciprocal process is expected, i.e., the spin-dependent Peltier effect. Flipse et al. [51] have recently reported the observation of this effect.

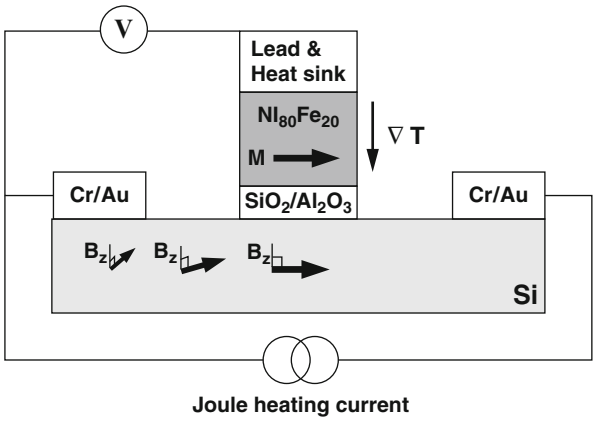

Fig. 9 Schematic of the Seebeck spin tunneling device reported in Ref. [17]. The silicon strip is heated by Joule dissipation, yielding $T_{Si} > T_{NiFe}$. Thermally induced spin accumulation in the silicon strip is detected by the Hanle effect

Seebeck Effect in Magnetic Tunnel Junctions

The tunneling magneto-thermopower ratio of magnetic tunnel junctions, which was discussed analytically [52] and computed by a first-principle calculation [53], has been measured by several groups. Walter et al. [54] and Liebing et al. [55] observed the tunneling magneto-thermopower in a CoFe/MgO/CoFe magnetic tunnel junction. The signal is caused by the spin-dependent Seebeck effect.

Magnon-Drag Thermopile

It has been well known that in magnetic metals, two drag effects contribute to the thermoelectric effect: one is the phonon-drag process in which the momentum transfer occurs from nonequilibrium phonons to conduction electrons and produces thermopower, and the other is the magnon-drag process in which the momentum transfer occurs from nonequilibrium magnons to conduction electrons [56]. However, the magnon-drag effect is easily masked by the phonon-drag effect, and in general, it is quite difficult to investigate only the magnon-drag effect. Costache et al. [57] recently overcame this difficulty and proposed a device named the "magnon-drag thermopile" which provides information about the magnon-drag effect. The device is shown in Fig. 10 where a large number of pairs of NiFe wires are connected electrically in series with Ag wires but placed thermally in parallel. When the two magnetizations in a pair of NiFe wires are in the parallel configuration, the thermopower is zero because the contributions of each wire are of the same magnitude but opposite signs. However, when the two magnetizations in a pair of NiFe wires are in the antiparallel configuration, there is a difference in the magnon states between the two wires, and the resultant thermopower is nonzero. Note that, in principle, although any electron-magnon scattering process other than the magnon-drag process can contribute to the observed thermopower, the magnon-drag process can dominate the signal when the energy dependence of the electron lifetime can be neglected.

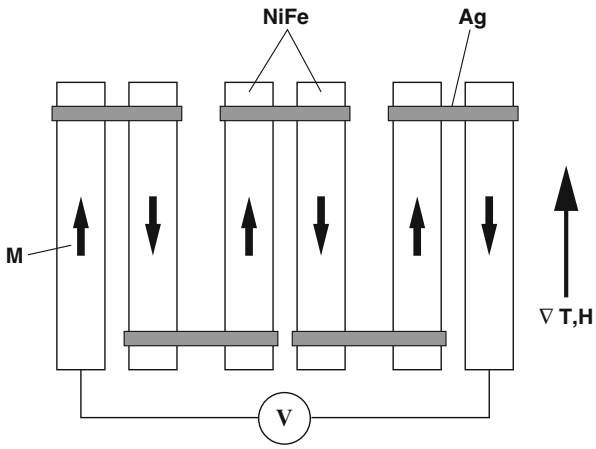

Fig. 10 Schematic of the magnon-drag thermopile proposed in Ref. [57]. A large number of pairs of NiFe wires are connected electrically in series with Ag wires

Thermal Spin-Transfer Torque

Thermal spin-transfer torque is also a highly debated topic. Hatami et al. [58] discussed the thermal spin-transfer torque in magnetic nanostructures of metals, and Jia et al. [59] recently developed a first-principle estimation of the same process. This effect is relevant to the thermally driven domain wall motion discussed analytically by Kovalev et al. [60] and computed numerically by Yuan et al. [61]. Thermal spin-transfer torque has also been discussed in the context of magnetic insulators. Slonczewski [62] discussed the thermal spin-transfer torque resulting from the longitudinal spin Seebeck effect in ferrite. Hinzke et al. [63] discussed the role of magnonic thermal spin-transfer torque. Experimentally, an evidence for the thermal spin-transfer torque was reported by Yu et al. [64].

Thermally Driven Spin-Wave Amplification

Another interesting subject is the dynamics of magnon wave packets under the influence of a temperature gradient. Padrón-Hernández et al. [65] found that magnon wave packets propagating along an yttrium iron garnet film are amplified when a temperature gradient is applied perpendicular to the yttrium iron garnet film (Fig. 11). This experiment implies that the magnon damping term is canceled by the action of the temperature gradient, which leads to an amplification of the magnon wave packet. The observed result was interpreted by the authors in terms of the magnonic spin-transfer torque [63, 66] in the longitudinal spin Seebeck effect configuration.

Anomalous Nernst Effect

The anomalous Nernst effect refers to the generation of a voltage gradient $\nabla V \parallel \hat{m} \times \nabla$ by applying a temperature gradient ∇ in a ferromagnetic material with a

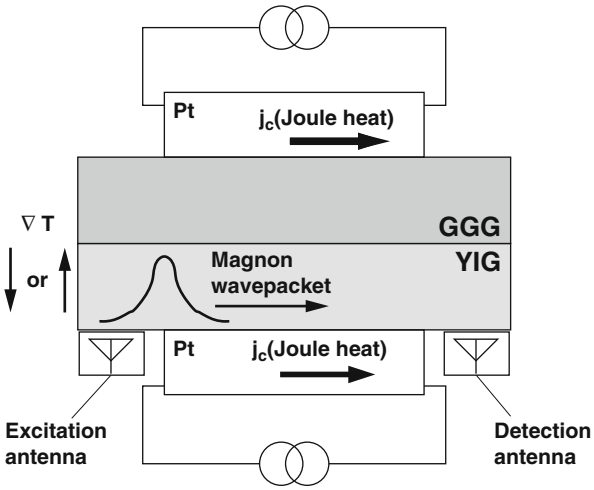

Fig. 11 Schematic of the experimental setup for the thermal-driven spin-wave amplification reported in Ref. [65]. A temperature gradient is applied to a hybrid system of yttrium iron garnet (*YIG*) and gadolinium gallium garnet (*GGG*) using the Joule heating in either of the attached Pt films

magnetic polarization vector $\hat{m}$. This phenomenon has been studied systematically in various ferromagnetic metals by Miyasato et al. [67], in (Ga, Mn)As by Pu et al. [68], and in $Ni_{80}Fe_{20}$ lateral spin valve by Slachter et al. [69]. It is important to note that if a thermal conductivity mismatch between the substrate and the ferromagnetic film exists when measuring the transverse spin Seebeck effect in the case of a *conducting* magnet, there can be a parasitic contribution from the anomalous Nernst effect as pointed out in Ref. [20]. This issue was recently discussed again in Ref. [70]. Quite recently, Chien and collaborators argued that the longitudinal SSE in a Pt/insulating magnet hybrid system is contaminated by the anomalous Nernst effect because of a strong magnetic proximity effect of Pt at the Pt/insulating magnet interface [71].

Thermal Hall Effect of Phonons and Magnons

When the time-reversal symmetry is broken by a magnetic field or a magnetic ordering, a finite Hall response can occur in principle even in the case of charge-neutral excitations such as phonons and magnons. Recently, the thermal Hall effect of phonons and magnons has been reported. Strohm et al. observed the thermal Hall effect of phonons in a paramagnetic insulator of terbium gallium garnet [72]. The result was explained by the interaction of local magnetic ions with the local orbital angular momentum of oscillating surrounding ions [73, 74]. The thermal Hall effect of magnons was also observed in an insulating ferromagnet $LU_2V_2O_7$ with pyrochlore structure [75], and the result was explained in terms of a Dzyaloshinskii-Moriya interaction. The Hall effect of magnons was also discussed theoretically in Refs. [76–78].

Summary

The physics of the spin Seebeck effect has been discussed as well as a brief summary of other thermospin phenomena has been presented in which the interplay of spin and heat is of importance. Regarding the spin Seebeck effect, the important role played by nonequilibrium magnons and phonons has been clarified. From a theoretical viewpoint, one of the open questions in the spin Seebeck effect is the role of spin-polarized conduction electrons in the metallic and semiconducting ferromagnets, especially in interpreting the experiment reported in Ref. [79]. From an experimental viewpoint, on the other hand, one of the most challenging issues is clarifying to what extent the spin Seebeck effect can be applied. A small but a firm step is already in progress [80–82].

More generally, one of the driving forces for investigating thermal effects in spintronics is the desire to deal with heating problems in modern solid-state devices. From this viewpoint, the thermo-spintronics is still in its infancy, and many issues still remain unclear. For example, the relationship between the pure spin current and dissipation [83] needs to be investigated extensively. Although the practical application of thermo-spintronics looks remote at present, it can be definitely said that the interplay of spin and heat manifests itself in state-of-the-art experiments and involves interesting physics.

Acknowledgments We are grateful for the fruitful discussions with E. Saitoh, K. Uchida, S. Takahashi, J. Ohe, J. P. Heremans, and G. E. W. Bauer. This study was supported by a Grant-in-Aid for Scientific Research from MEXT, Japan.

References

1. Kondo J (1965) Giant thermo-electric power of dilute magnetic alloys. Prog Theor Phys 34:372–382
2. Maekawa S, Kashiba S, Tachiki M, Takahashi S (1986) Thermopower in Ce Kondo systems. J Phys Soc Jpn 55:3194–3198
3. Takabatake T, Sasakawa T, Kitagawa J, Suemitsu T, Echizen Y, Umeo K, Sera M, Bando Y (2003) Thermoelectric properties of Ce-based Kondo semimetals and semiconductors. Physica B 328:53–57
4. Callen HB (1948) The application of Onsager's reciprocal relations to thermoelectric, thermomagnetic, and galvanomagnetic effects. Phys Rev 73:1349–1358
5. Johnson M, Silsbee RH (1987) Thermodynamic analysis of interfacial transport and of the thermomagnetoelectric system. Phys Rev B 35:4959–4972
6. Sakurai J, Horie H, Araki S, Yamamoto H, Shinjo T (1991) Magnetic field effects on thermopower of Fe/Cr and Cu/Co/Cu/Ni(Fe) multilayers. J Phys Soc Jpn 60:2522–2525
7. Conover MJ, Brodsky MB, Mattson JE, Sowers CH, Bader SD (1991) Magnetothermopower of Fe/Cr superlattices. J Magn Magn Mater 102:L5–L8
8. Piraux L, Fert A, Schroeder PA, Loloee R, Etienne P (1992) Large magneto-thermoelectric power in Co/Cu, Fe/Cu and Fe/Cr multilayers. J Magn Magn Mater 110:L247–L253

9. Shi J, Pettit K, Kita E, Parkin SSP, Nakatani R, Salamon MB (1996) Field-dependent thermoelectric power and thermal conductivity in lultilayered and granular giant magnetoresistive systems. Phys Rev B 54:15273–15283
10. Baily S, Salamon MB, Oepts W (2000) Magnetothermopower of cobalt/copper multilayers with gradient perpendicular to planes. J Appl Phys 87:4855–4857
11. Wegrowe JE (2000) Thermokinetic approach of the generatized Landau-Lifshitz-Gilbert equation with spin-polarized current. Phys Rev B 62:1067–1074
12. Fukushima A, Yagami K, Tulapurkar AA, Suzuki Y, Kubota H, Yamamoto A, Yuasa A (2005) Peltier effect in sub-micron-size metallic junctions. Jpn J Appl Phys 44:L12–L14
13. Gravier L, Serrano-Guisan S, Reuse F, Ansermet JP (2006) Thermodynamic description of heat and spin transport in magnetic nanostructures. Phys Rev B 73:024419
14. Tsyplyatyev O, Kashuba O, Fal'ko VI (2006) Thermally excited spin current and giant magnetothermopower in metals with embedded ferromagnetic nanoclusters. Phys Rev B 74:132403
15. Dubi Y, Ventra MD (2009) Thermospin effects in a quantum dot connected to ferromagnetic leads. Phys Rev B 79:081302
16. Slachter A, Bakker FL, Adam JP, van Wees BJ (2010) Thermally driven spin injection from a ferromagnet into a non-magnetic metal. Nat Phys 6:879–883
17. Le Breton J, Sharma S, Saito H, Yuasa S, Jansen R (2011) Thermal spin current from a ferromagnet to silicon by Seebeck spin tunneling. Nature 475:82–85
18. Uchida K, Takahashi S, Harii K, Ieda J, Koshibae W, Ando K, Maekawa S, Saitoh E (2008) Observation of the spin Seebeck effect. Nature 455:778–781
19. Bauer GEW, Saitoh E, van Wees BJ (2012) Spin caloritronics. Nat Mater 11:391–399
20. Bosu S, Sakuraba Y, Uchida K, Saito K, Ota T, Saitoh E, Takanashi K (2011) Spin Seebeck effect in thin films of the Heusler compound Co_2MnSi. Phys Rev B 83:224401
21. Jaworski CM, Yang J, Mack S, Awschalom DD, Heremans JP, Myers RC (2010) Observation of the spin-Seebeck effect in a ferromagnetic semiconductor. Nat Mater 9:898–903
22. Uchida K, Xiao J, Adachi H, Ohe J, Takahashi S, Ieda J, Ota T, Kajiwara Y, Umezawa H, Kawai H, Bauer GEW, Maekawa S, Saitoh E (2010) Spin Seebeck insulator. Nat Mater 9:894–897
23. Uchida K, Nonaka T, Ota T, Nakayama H, Saitoh E (2010) Longitudinal spin-Seebeck effect in sintered polycrystalline (Mn, Zn)Fe_2O_4. Appl Phys Lett 97:262504
24. Saitoh E, Ueda M, Miyajima H, Tatara G (2006) Conversion of spin current into charge current at room temperature: inverse spin-Hall effect. Appl Phys Lett 88:182509
25. Hatami M, Bauer GEW, Takahashi S, Maekawa S (2010) Thermoelectric spin diffusion in a ferromagnetic metal. Solid State Commun 150:480–484
26. Nunner TS, von Oppen F (2011) Quasilinear spin-voltage profiles in spin thermoelectrics. Phys Rev B 84:020405, Nunner *et al*. argued that an inclusion of an inelastic spin flip scattering could give longer length scales for conduction electrons
27. Kajiwara Y, Harii K, Takahashi S, Ohe J, Uchida K, Mizuguchi M, Umezawa H, Kawai H, Ando K, Takanashi K, Maekawa S, Saitoh E (2010) Transmission of electrical signals by spin-wave interconversion in a magnetic insulator. Nature 464:262–266
28. Maekawa S (ed) (2006) Concepts in spin electronics. Oxford University Press, Oxford
29. Brown WF Jr (1963) Thermal fluctuations of a single-domain particle. Phys Rev 130:1677–1686
30. Zhang S, Li Z (2004) Roles of nonequilibrium conduction electrons on the magnetization dynamics of ferromagnets. Phys Rev Lett 93:127204
31. Ma S, Mazenko GF (1975) Critical dynamics of ferromagnets in 6-ε dimensions: general discussion and detailed calculation. Phys Rev B 11:4077–4100
32. Kubo R, Toda M, Hashitsume N (1991) Statistical physics II: nonequilibrium statistical mechanics. Springer, Heidelberg
33. Tserkovnyak Y, Brataas A, Bauer GEW, Halperin BI (2005) Nonlocal magnetization dynamics in ferromagnetic heterostructures. Rev Mod Phys 77:1375–1421

34. Foros J, Brataas A, Tserkovnyak Y, Bauer GEW (2005) Magnetization noise in magnetoelectronic nanostructures. Phys Rev Lett 95:016601 (1–4)
35. Ohe J, Adachi H, Takahashi S, Maekawa S (2010) Numerical study on the spin Seebeck effect. Phys Rev B 83:115118
36. Xiao J, Bauer GEW, Uchida K, Saitoh E, Maekawa S (2010) Theory of magnon-driven spin Seebeck effect. Phys Rev B 81:214418
37. Adachi H, Ohe J, Takahashi S, Maekawa S (2011) Linear-response theory of spin Seebeck effect in ferromagnetic insulators. Phys Rev B 83:094410
38. Adachi H, Uchida K, Saitoh E, Ohe J, Takahashi S, Maekawa S (2010) Gigantic enhancement of spin Seebeck effect by phonon drag. Appl Phys Lett 97:252506
39. Sanders DJ, Walton D (1977) Effect of magnon-phonon thermal relaxation on heat transport by magnons. Phys Rev B 15:1489–1494
40. Ussishkin I, Sondhi SL, Huse D (2002) Gaussian superconducting fluctuations, thermal transport, and the nernst effect. Phys Rev Lett 89:287001
41. Ma SK (1976) Modern theory of critical phenomena. Benjamin/Cummings, Reading
42. Hohenberg PC, Shraiman BI (1989) Chaotic behavior of an extended system. Physica D 37:109–115
43. Chaikin PM, Lubensky TC (1995) Principles of condensed matter physics. Cambridge University Press, Cambridge
44. Vittoria C, Lubitz P, Hansen P, Tolksdorf W (1985) FMR linewidth measurements in bismuth-substituted YIG. J Appl Phys 57:3699–3700
45. Jaworski CM, Yang J, Mack S, Awschalom DD, Myers RC, Heremans JP (2011) Spin-Seebeck effect: a phonon driven spin distribution. Phys Rev Lett 106:186601
46. Uchida K, Ota T, Adachi H, Xiao J, Nonaka T, Kajiwara Y, Bauer GEW, Maekawa S, Saitoh E (2011) Thermal spin pumping and magnon-phonon-mediated spin-Seebeck effect. J Appl Phys 111:103903
47. Uchida K, Adachi H, An T, Ota T, Toda M, Hillebrands B, Maekawa S, Saitoh E (2011) Long-range spin Seebeck effect and acoustic spin pumping. Nat Mater 10:737–741
48. Uchida K, Adachi H, Ota T, Nakayama H, Maekawa S, Saitoh E (2010) Observation of longitudinal spin-Seebeck effect in magnetic insulators. Appl Phys Lett 97:172505
49. Adachi H, Maekawa S (2013) Linear-response theory of the longitudinal spin Seebeck effect. J Korean Phys Soc 62:1753–1758
50. Slack GA, Oliver DW (1971) Thermal conductivity of garnets and phonon scattering by rare-earth ions. Phys Rev B 4:592
51. Flipse J, Bakker FL, Slachter A, Dejene FK, van Wees BJ (2012) Direct observation of the spin-dependent Peltier effect. Nat Nanotechnol 7:166–168
52. Hatami M, Bauer GEW, Zhang QF, Kelly PJ (2009) Thermoelectric effects in magnetic nanostructures. Phys Rev B 79:174426
53. Czerner M, Bachmann M, Heiliger C (2011) Spin caloritronics in magnetic tunnel junctions: Ab initio studies. Phys Rev B 83:132405 (1–4)
54. Walter M, Walowski J, Zbarsky V, Münzenberg M, Schäfers M, Ebke D, Reiss G, Thomas A, Peretzki P, Seibt M, Moodera JS, Czerner M, Bachmann M, Heiliger C (2011) Seebeck effect in magnetic tunnel junctions. Nat Mater 10:742–746
55. Liebing N, Serrano-Guisan S, Rott K, Reiss G, Langer J, Ocker B, Schumacher HW (2011) Tunneling magnetothermopower in magnetic tunnel junction nanopillars. Phys Rev Lett 107:177201
56. Blatt FJ, Schroeder PA, Foiles CL, Greig D (1976) Thermoelectric power of metals. Plenum Press, New York
57. Costache MV, Bridoux G, Neumann I, Valenzuela SO (2011) Magnon-drag thermopile. Nat Mater 11:199–202
58. Hatami M, Bauer GEW, Zhang QF, Kelly PJ (2007) Thermal spin-transfer torque in magnetoelectronic devices. Phys Rev Lett 99:066603

59. Jia X, Xia K, Bauer GEW (2011) Thermal spin transfer in Fe-MgO-Fe tunnel junctions. Phys Rev Lett 107:176603
60. Kovalev AA, Tserkovnyak Y (2009) Thermoelectric spin transfer in textured magnets. Phys Rev B 80:100408
61. Yuan Z, Wang S, Xia K (2010) Thermal spin-transfer torques on magnetic domain walls. Solid State Commun 150:548–551
62. Slonczewski JC (2010) Initiation of spin-transfer torque by thermal transport from magnons. Phys Rev B 82:054403
63. Hinzke D, Nowak U (2011) Domain wall motion by the magnonic spin Seebeck effect. Phys Rev Lett 107:027205
64. Yu H, Granville S, Yu DP, Ansermet JP (2010) Evidence for thermal spin-transfer torque. Phys Rev Lett 104:146601
65. Padrón Hernández E, Azevedo A, Rezende SM (2011) Amplification of spin waves by thermal spin-transfer torque. Phys Rev Lett 107:197203
66. Yan P, Wang XS, Wang XR (2011) All-Magnonic spin-transfer torque and domain wall propagation. Phys Rev Lett 107:177207
67. Miyasato T, Abe N, Fujii T, Asamitsu A, Onoda S, Onose Y, Nagaosa N, Tokura Y (2007) Crossover behavior of the anomalous Hall effect and anomalous nernst effect in itinerant ferromagnets. Phys Rev Lett 99:086602
68. Pu Y, Chiba D, Matsukura F, Ohno H, Shi J (2008) Mott relation for anomalous Hall and Nernst effects in $Ga_{1-x}Mn_xAs$ ferromagnetic semiconductors. Phys Rev Lett 101:117208
69. Slachter A, Bakker FL, van Wees BJ (2011) Anomalous Nernst and anisotropic magnetoresistive heating in a lateral spin valve. Phys Rev B 84:020412(R)
70. Huang SY, Wang WG, Lee SF, Kwo J, Chien CL (2011) Intrinsic spin-dependent thermal transport. Phys Rev Lett 107:216604
71. Huang SY, Fan X, Qu D, Chen YP, Wang WG, Wu J, Chen TY, Xiao JQ, Chien CL (2012) Transport magnetic proximity effects in platinum. Phys Rev Lett 109:107204
72. Strohm C, Rikken GLJA, Wyder P (2005) Phenomenological evidence for the phonon Hall effect. Phys Rev Lett 95:155901
73. Sheng L, Sheng DN, Ting CS (2006) Theory of the phonon Hall effect in paramagnetic dielectrics. Phys Rev Lett 96:155901
74. Kagan Y, Maksimov LA (2008) Anomalous Hall effect for the phonon heat conductivity in paramagnetic dielectrics. Phys Rev Lett 100:145902
75. Onose Y, Ideue T, Katsura H, Shiomi Y, Nagaosa N, Tokura Y (2010) Observation of the magnon Hall effect. Science 329:297
76. Fujimoto S (2009) Hall effect of spin waves in frustrated magnets. Phys Rev Lett 103:047203
77. Katsura H, Nagaosa N, Lee PA (2010) Theory of the thermal Hall effect in quantum magnets. Phys Rev Lett 104:066403
78. Matsumoto R, Murakami S (2011) Theoretical prediction of a rotating magnon wave packet in ferromagnets. Phys Rev Lett 106:197202
79. Jaworski CM, Myers RC, Johnston-Halperin E, Heremans JP (2012) Giant spin Seebeck effect in a non-magnetic material. Nature 487:210–213
80. Kirihara A, Uchida K, Kajiwara Y, Ishida M, Nakamura Y, Manako T, Saitoh E, Yorozu S (2012) Spin-current-driven thermoelectric coating. Nat Mater 11:686–689
81. Uchida K, Kirihara A, Ishida M, Takahashi R, Saitoh E (2011) Local spin-Seebeck effect enabling two-dimensional position sensing. J Appl Phys 50:120211
82. Uchida K, Nonaka T, Yoshino T, Kikkawa T, Kikuchi D, Saitoh E (2012) Enhancement of spin-Seebeck voltage by spin-Hall thermopile. Appl Phys Express 5:093001
83. Tulapurkar AA, Suzuki Y (2011) Boltzmann approach to dissipation produced by a spin-polarized current. Phys Rev B 83:012401